Al-Nahrain Journal for Engineering Sciences **NJES** 25(1)35-43, 2022
http://doi.org/10.29194/NJES.25010035

Hydrodynamics of Stirred Tank and Bubble Breakup Behavior Induced by Rushton Turbine

Anas M. Mhawesh[*1], Basim O. Hasan[2], Hussein Znad[3]

Authors affiliations:
1) Chemical Engineering Department, Al-Nahrain University, Iraq.
anasmalik969@gmail.com

2) Chemical Engineering Department, Al-Nahrain University, Iraq.
basimhasan2017@eng.nahrainuniv.edu.iq

3) WA School of Mines: Minerals, Energy and Chemical Engineering, Curtin University, Perth, WA, 6845, Australia.
H.Znad@curtin.edu.au

Paper History:

Received: 7th Dec. 2021

Revised: 31st Dec. 2021

Accepted: 11th Jan. 2022

Abstract

The hydrodynamics of stirred tanks and bubble breakup are crucial in gas-liquid flows, yet this system has not been well characterized for different operating conditions. In this work, the numerical method was used to investigate the hydrodynamics of six- flat blades impeller (Rushton turbine) and the results were employed to understand the bubble breakup behavior in the stirred tank. Simulation results of predicted flow pattern, power number, and the distribution of turbulence energy generated were performed with COMSOL Multiphysics. Numerical results showed good agreement with the experimental literature. The effect of rotational speed on bubble breakup behavior, such as breakage probability, the average number of daughter bubbles, and the breakage time was investigated using the high-speed imaging method. The main finding is that the breakage process occurs in the high energy area of high turbulence intensity, which is located within a distance equal to the blade width of a radius of (15-35 mm). The breakage probability (Bp) was found to be increased by 12.61 percent for a mother bubble of 4 mm at 340 rpm, with an average fragmentation of up to 22 fragments. Furthermore, the bubble breakage time was found to decrease with increasing impeller rotational speed, with an average value of 19.8 ms.

Keywords: Stirred tank, Rushton turbine, CFD, Bubble breakup, Breakup time.

هيدروديناميكا خزان الخلط وسلوك تفكك الفقاعات الناجم عن توربين راشتون

انس مالك محاوش ، باسم عبيد حسن ، حسين زناد

الخلاصة:

تعتبر هيدروديناميكا خزانات الخلط وتفكك الفقاعات أمرًا بالغ الأهمية في تدفقات الغاز والسائل ، ومع ذلك لم يتم تشخيص وتوصيف هذا النظام جيدًا لظروف التشغيل المختلفة. في هذا العمل ، تم استخدام الطريقة العددية لاستقصاء الديناميكا المائية لمكره الشفرات الست المسطحة (توربين رشتون) وتم استخدام النتائج لفهم سلوك تكسير الفقاعات في خزان الخلط. تم إجراء نتائج محاكاة نمط التدفق المتوقع ورقم الطاقة وتوزيع طاقة الاضطراب المتولدة باستخدام COMSOL Multiphysics. أظهرت النتائج العددية توافق جيد مع الاعمال التجريبية. تم دراسة تأثير سرعة الدوران على سلوك تكسير الفقاعات مثل احتمالية الكسر ومتوسط عدد الفقاعات الوليدة ووقت الكسر باستخدام طريقة التصوير عالي السرعة. الاكتشاف الرئيسي هو أن عملية الكسر تحدث في منطقة عالية الطاقة ذات شدة اضطراب عالية ، والتي تقع ضمن مسافة مساوية لعرض الشفرة في نصف قطر (١٥-٣٥ مم). تم العثور على زيادة احتمال الكسر (Bp) بنسبة ١٢,٦١ في المائة للفقاعة الأم التي يبلغ قطرها ٤ مم عند ٣٤٠ دورة في الدقيقة ، بمتوسط تجزئة يصل إلى ٢٢ شظية. علاوة على ذلك ، وجد أن وقت كسر الفقاعة يتناقص مع زيادة سرعة دوران التوربين، بمتوسط قيمة ١٩,٨ ملي ثانية.

1. Introduction

Chemical engineering involves both physical and chemical process which are employed to convert the raw materials into useful products. On the industrial scale, the main chemical processes involve mixing and reaction of one substance with another [1]. Process industries contain many sectors that involve the use of gas-liquid and liquid-liquid multiphase flows where the breakage of fluid particles plays an important role, including the petroleum, food and pharmaceutical industries., chemical reaction in the liquid,

NJES is an **open access Journal** with **ISSN 2521-9154** and **eISSN 2521-9162**
This work is licensed under a Creative Commons Attribution-NonCommercial 4.0 International License

hydrogenations, oxidations, and bioprocess fermentations [2].

Dispersion is the process of creation suspended (gas, liquid, and solid) particles in an immiscible fluid and typically used to improve the mass or heat transfer of a component from phase to liquid and vice versa [3]**.** Dispersion is caused by high shear mixers, which transport a lot of turbulent energy to the system. Turbulence caused by this energy disperses the gas bubbles throughout the liquid phase by breaking them into small bubbles. As a result of this, the contact area which is a n important industrial parameter between the gas and the liquid is increased [4]. Due to the flexibility of mechanically stirred vessels, made it a commonly used equipment in the industry and one of most common devices used to improve the dispersion process in which the gas is injected at the bottom and dispersed by stirring impeller where it produces higher mass transfer rates.

1.2 Bubble break-up

A bubble break-up results into two or more generated bubbles, and the interfacial area increases and so does the interfacial transfer between phases. The break-up process can be expressed as the balance between hydrodynamic forces and surface tension forces and form Weber number [5][6].

Therefore, different mechanisms of the bubbles break-up are exist depending on the flow region hydrodynamic.

In turbulent fluid, the break-up is occurring due to bubble-eddy collisions. In laminar flow, the viscous shear at the bubble surface will elongate the bubble and cause break-up by velocity gradient. An additional break-up mechanism that is common in natural and industrial processes, fluid particles may break in stagnant fluid due to density differences causing interfacial instabilities.

1.3 Turbulent break-up mechanism

In turbulent condition which is the case likely happening in stirred tanks, kinetic energy in form of random fluctuations in velocity (known as eddies) is the main mechanism for bubble breakup [7]. The size of greatest eddies will be proportionate to the size of the equipment that creates the flow (for example, the blade width). The Kolmogorov scale (λo), on the other hand, represents the size of the smallest eddies. Because of this the larger eddies exist for a longer period of time than the smaller ones, this knowledge is crucial to the effective design and scaleup of mixing processes [7][8]. The size of eddies formed is employed to distinguish the regime in turbulent condition resulting in two basic regions 'turbulent inertial regime' and 'turbulent viscous regime' as shown in Fig.1. The droplets/bubbles in the turbulent inertia regime are larger than the smallest turbulent eddies[5]. The opposite is in the turbulent viscous regime, where the bubble is smaller than the size of the smallest eddies [9]. In addition to the size of eddies, the contact period between a bubble and turbulent eddies is efficient in causing a breakage [10]. The energy of eddies that has length scales equal or lower than fluid particle diameter will break the drop or bubble, while larger eddies simply transport them [5][10][11]. To capture the effect of eddies it is normally approximated by terms of the turbulent energy dissipation rate per unit mass, ε [11].

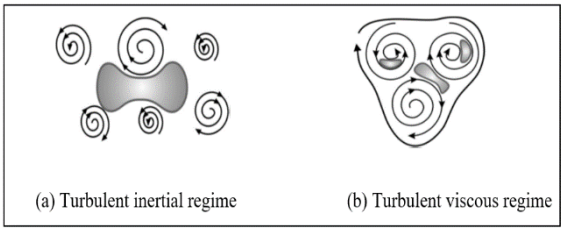

Figure 1: Presentation of two different turbulent regime.

Hasan (2017) made a good review of the existing particles (droplets and bubbles) breakage mechanisms in stirred tanks. Three primary mechanisms are proposed as a result of his research [10]:

(i) Particle–eddy collisions: In the bulk region, the particle deforms and breaks up due to collision with the turbulent eddies that generated or transported from the flow of the impeller discharge region.

(ii) Shear of the blade: In the impeller region at the boundary layer covers the front side of the blades surface and the trailing vortex, the particle deforms and breaks up as a result of the shear effects generated from the difference between the gases velocity inside the particles and the velocity of the liquid flow at the particle-fluid interface.

(iii) particle-blade collision: The collision between the fluid particle and the blade has been observed experimentally and can result in a breaking without or with small deformation, depending on the blade geometry and agitation speed

Thus, the hydrodynamics and the distribution of the turbulent kinetic energy dissipation rate has a major effect in determining the success of dispersion process and the breakage rate as well as the stable bubble size [12][5]. Mixing increases the break-up rate which is necessary to build and solve the population balance model (PBM) and knowing the bubble size distribution. And therefore, increasing the interfacial area of dispersion and reaction rate and products yield. As discussed by Solsvik [13] and Liao and Lucas [14], a number of bubble break-up models have been proposed. However, because reliable bubble break-up experimental data is limited, evaluating the accuracy of bubble break-up models is difficult.

This work aimed to investigate the hydrodynamics of stirred tank of six-flat blades Rushton turbine by CFD simulation and characterize the bubble breakage behavior. The effect of rotational speed was investigated by determining the breakage probability, average daughter bubbles generated by using a high-speed imaging technique.

2.1 Experimental materials and setup

The experiments were conducted at the laboratories of Department of Chemical Engineering/ Al-Nahrain University. As shown in Fig. 2, the system

consists of a cylindrical flat bottom tank partially baffled made from transparency material (acrylic glass) filled with water as a continuous phase. The stirrer is equipped with the acrylic shaft attached to Rushton turbine (6RT). To avoid optical distortions, the cylindrical tank is placed in a square glass tank (360*360*360 mm). An air pump of the model (RS Electrical Silent Aquarium air pump RS-628A with two outlets) this type is available, cheap and at the same time very practical, is connected to a Teflon tube for injecting the bubble centered below the impeller. A plastic tube was used to surround the injection tube to protect the bubbles during the formation stage and prevent the bubble from detaching earlier. Table 1 shows the dimensions of the stirred tank and the injection system.

A plastic ball valve (inner diameter 6.3 mm) was used to ensure a constant airflow rate (Q) during the injection of the mother bubble. A high-speed camera (Phantom Miro-C110) was used with a resolution of the images of 1280×800 pixel and the recording speed at this resolution 1200 frames per second (fps) at full resolution. LED of 300 Watt for illumination and Tachometer for calibration of the stirrer rotational speeds. The experiments were conducted at room temperature.

Table 1: Geometrical parameters of the stirred tank.

Parameter	Value
Tank height, H, mm	400
Tank diameter, T, mm	180
Height of liquid surface, Ls, mm	H
Injection distance below the impeller, Δh, mm	35
Number of baffles, Nj	2
Baffle width, mm	18
Impeller diameter, Di, mm	70
Width of blade, W, mm	20
Length of blade, L, mm	20
Shaft diameter, Ds, mm	20
Impeller disc diameter, Dc, mm	40
Injection tube diameter, mm	4

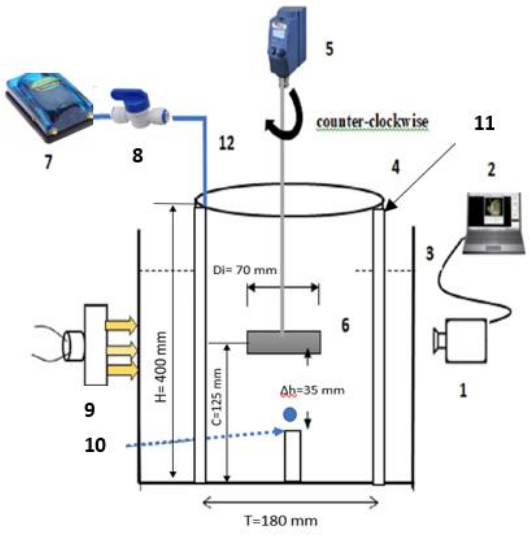

Figure 2: Experimental setup, 1-high speed camera, 2-computer, 3-outer glass tank, 4-inner cylindrical tank, 5-stirrer, 6-impeller, 7-air pump, 8-gas control valve, 11-LED lamp, 10- injection tube, 11-baffle.

2.2 Experimental procedures

The experiment was conducted in stirred tanks with two baffles. The impeller made from transparent acrylic material, which reveals the changes and behavior of the bubble in the impeller's highly turbulence area and indicates the number of fragments bubble produced for each breakage. Impeller was located at a clearance of 35 mm above the injection position of mother bubble.

A mechanical gas valve was utilized to control the injection rate, as a consequence, injected bubbles develop and enter the high non-uniform turbulence generated by the impellers. Due to the high rotating flow currents in the tank, the injected bubble would frequently detach from the sparger pipe before reaching the desired size. The injected bubble size has to be regulated for the range of stirring speed adopted in order to examine the effect of increasing stirring speed. An exterior plastic tube was utilized to frame the sparger pipe to overcome this problem. The outer tube protected the injected bubble from the flow currents and finally reached its full size [15][16]. The frame tube had a diameter of 10 mm. The inside diameter of the injection pipe was 4mm, and the stable diameter of injected bubbles was approximately 4 mm for the range of investigated rotational speed.

Because the injection position affects the bubble's trajectory [17][18], the sparger pipe was placed beneath the impeller in center of the tank's bottom, where the majority of injected bubbles can reach the impeller region.

Each experiment captured at least 500 bubbles by injecting the bubbles one by one. For low rotational speed, an average of one bubble was injected every 4 seconds. As a result of the large number of fragments created, and their buoyancy force, a slower injection rate was employed for higher rotational speeds.

ImageJ, an open-source program, was used to analyze high-speed images of mother bubbles that had broken. As seen in Fig. 3, image processing techniques included background noise removal, thresholding, and outline tracking to determine bubble size (diameter). For size reference items, the blade dimension or any known distance was employed. The diameter obtained from the two-dimensional image was used to express the size of each bubble.

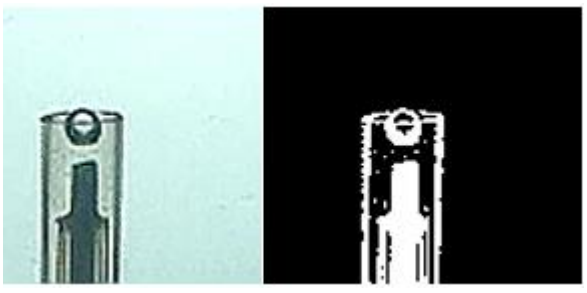

Figure 3: Post processing of the pierced bubble using ImageJ software.

3. Computational approach

3.1 Geometry

The hydrodynamics generation in the system were studied using software COMSOL Multiphysics 5.5. As the setup is shown in Fig. 4, the flow field was investigated in a cylindrical tank with a height of H=400mm and a diameter of T=180mm. Two symmetrical baffles were equipped width of W = 0.1 T to avoid vortex formation on the free surface. Water is the working medium with density of (ϱ= 998 kg/m^3) and viscosity of (μ = 0.001 Pa·s).

The effects of rotational speed on hydrodynamics in the tank were investigated. Simulations were performed on a Lenovo Idea-pad 320 PC intel i7CPU with **8** GB memory.

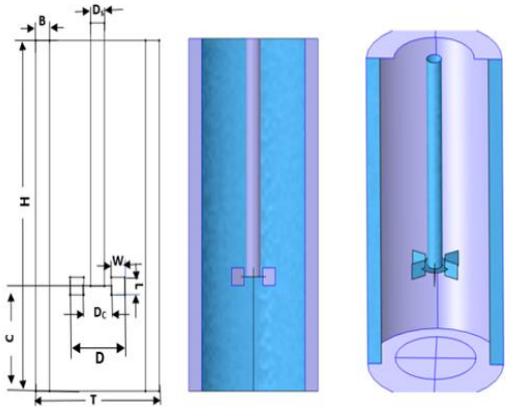

Figure 4: Schematic diagram of the stirred tank.

3.2 Mathematical model

In order to simulate the turbulent flow in the stirred tank, partial differential equations (PDEs) are used to describing the conservation of mass and momentum within the flow system. The continuity equation describes the mass conservation [19][20]:

$$\frac{\partial \rho}{\partial t} + \nabla\,(\varrho \cdot u) = 0 \qquad ...(1)$$

Reynolds averaged Navier-Stokes's (RANS) equations are used to describe the momentum conservation [19][20]:

$$\rho\frac{\partial u}{\partial t} + \rho(u\cdot\nabla)u = \nabla.[-pI + (\mu + \mu_T)(\nabla u + \nabla u^T) - \frac{2}{3}(\mu+\mu_T)(\nabla u)I - \frac{2}{3}\rho kI] + f \qquad ...(2)$$

Where u represent the velocity of flow, and ϱ is the density of the fluid, p is the pressure, μ is the fluid viscosity, μ_T is the turbulent eddy viscosity and F is the body forces. In all numerical analysis, the accuracy of results that use Reynolds-averaged Navier–Stokes equations (RANS) to model the effect of eddies depends on the turbulence models used [21]. In CFD simulation of flow and among numerous turbulence models, the k-ε model is considered to have a good convergence rate and relatively low memory requirements and can handle various fluid flow conditions. Based on that, the k-ε was the most common model used characteristics for turbulent conditions [20].

The k-ε model and RANS calculating the velocity field by using turbulence viscosity [19][20]:

$$\mu_T = C_\mu \frac{\rho k^2}{\varepsilon} \qquad ...(3)$$

The term (k) refers to turbulent kinetic energy and describe the movement of large eddies [19]:

$$\rho\frac{\partial k}{\partial t} + \rho(u\cdot\nabla)k = \nabla[(\mu + \frac{\mu_T}{\sigma_k})\nabla k] + p_k - \rho\varepsilon \qquad ...(4)$$

The term (ε) refers to turbulent energy dissipation, and describe the energy dissipation of the small eddies [19]:

$$\rho\frac{\partial \varepsilon}{\partial t} + \rho(u\cdot\nabla)\varepsilon = \nabla[(\mu + \frac{\mu_T}{\sigma_\varepsilon})\nabla\varepsilon] + C_{\varepsilon_1}\frac{\varepsilon}{k}p_k - C_{\varepsilon_2}\rho\frac{\varepsilon^2}{k} \qquad ...(5)$$

The production rate of turbulence kinetic energy and due to less computations are needed the stress is calculated as average stresses described by the stress tensor (P_k) defined as [19]:

$$p_k = \mu_T\left[\nabla.u(\nabla u + \nabla u^T) - \frac{2}{3}\nabla\cdot u^2\right] - \frac{2}{3}\rho k\nabla.u \qquad ...(6)$$

The parameters used in standard k- ε model for both liquid and gas phases are as follows: Cμ=0.09, C_{ε_1}=1.44, C_{ε_2}=1.92, σ_k=1.0 and σ_ε=1.3.

3.3 Computational details

The simulated cell in this study selecting 3D component and the mixture model of (The Rotating-Machinery, and Turbulent-Flow k-ε Interface) supports the study of stationary and time-dependent studies. The following assumptions were made in order to lower the computational load without dramatically altering the simulation results:

- The hydrodynamics generated in a stirred tank doesn't affect by dispersed phase and single-phase fluid was examined.
- The turbulent of the system was computed using a frozen rotor, which is an example of a steady-state study.

Among the many methods that do not need the requirements of experimental impeller boundary conditions, multiple frame of reference (MRF) method has lowest shortcomings in the mixing simulations [22]. MRF is considered as the simplest approaches for multiple zones and steady-state approximation for modeling impeller rotation. In order to model a rotating motion using CFD simulation approach, the MRF divided the system into a static domain which is include the fixed parts (walls, and baffles) and rotation domain that includes rotating impellers. Models were built using COMSOL Multiphysics platform.

3.4 Boundary conditions

Based on the experiment, the inner domain rotates with various stirring speeds at 180, 240, 340 rpm. As for initial conditions we employ the following assumptions:

- The process takes place at a constant temperature of 20 °C.
- No-slip conditions (u=0) at all wall-fluid interfaces.

- The pressure points constraint (P=0) at the upper edge of the blade.

3.5 Mesh selection

The meshes are generated by COMSOL Multiphysics 5.5 software. As shown in Fig.5. Tetrahedral unstructured meshes were generated for the inner domain. Moreover, Impeller region (10% of tank volume) was meshed with half size of total grids generated for the tank volume with a higher resolution on the impeller blades and baffle walls where the velocity gradients are expected to be high. The number of elements and degree of freedom was selected to achieve acceptable results for less simulation time. General Minimal Residual Method (GMRES) is an iterative method used to solve a non-symmetric system of linear equations[23]. The solution was considered to be converged when the relative residuals was less than (10^{-4}) for all the simulations.

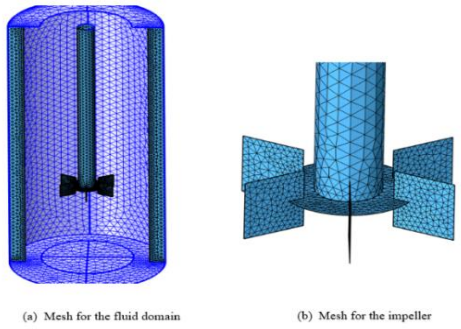

Figure 5: The mesh structure for the stirred tank built in COMSOL software.

3.4 Theoretical calculations

The mean energy dissipation rate has a nonuniformly distribution in stirred tanks, being much higher in impeller region than in the remainder of the fluid bulk. Therefore, the use of the total volume of the liquid is inaccurate in calculating the dissipated energy. Instead, assuming that most of the turbulent energy is in the region around the impeller, we get an alternative expression for (ε) [24]:

$$\varepsilon = \frac{p}{\rho\, D\text{^}3} \qquad ...(7)$$

The experimental data of more than 500 injected bubbles were gathered for determine the bubble breakup probability and the average number of produced fragments (N_{avr}). The bubble breakup probability Bp was determined as the percentage number of broken bubbles among the total injected bubbles.

The bubbles breakage probability is given by [11][17]:

$$Bp\% = \frac{\Sigma\ number\ of\ broken\ bubbles\ (Nb)}{\Sigma\ number\ of\ injected\ bubbles\ (Nt)} \times 100 \qquad ...(8)$$

The mean average number of generated bubbles is given by:

$$Navr = \frac{\Sigma\ bubbles\ produced}{\Sigma\ number\ of\ broken\ bubbles} \qquad ...(8)$$

4. Results and Discussion

4.1 Flow field pattern

The most common impeller and effective choice used in the bioindustry and gas dispersion processes is the six-flat blade disc turbine (Rushton turbine) shown in Fig. 6(a) [24]. The CFD simulation results are presented in this chapter. Fig.6(b) shows the radial flow patterns generated by the Rushton turbine used in the present work as in the vertical plots of the mean velocity vector. The discharged fluid flows horizontally from the blade tips and once the discharged fluid hits the wall tank, two symmetrical loops of circulated flow are formed. The arrows of mean velocity vector plot determine the direction and length of the velocity magnitude generated [24].

Most of the mixing and gas dispersion performance takes place near the impeller region [24]. Fig. 7 shows the intensity of dissipation rate of turbulence kinetic energy in stirred tank that associated with trailing vortices and described as randomly distributed. The formation of trailing vortices behind the blades of the impeller has consequences for phenomena such as fluid particle breakup and cell damage in bioreactors [24]. Horizontal plan Fig. 7(a), illustrates the covered area of turbulence kinetic energy dissipation rate with highest magnitude occurs at the blades tip in the discharged fluid leaving the blades as obtained by CFD simulation. It can be seen that it is maximum at the blade's tip and gradually decreasing toward the tank wall. Vertical plan Fig. 7(b), shows the weakly transmit of turbulence kinetic energy dissipation rate above or below the turbine. This trend of energy dissipation rate affects the dispersion of bubble/drop in two-phase flow processes. It can be seen that there is a relatively high level or energy dissipation at the wall due to the presence of baffles.

4.2 Effect of rotational speed

Fig. 8 in vertical plan shows the effect of rotational speed (N) on turbulence dissipation rate (ε) generated by Rushton turbine. Three rotational speeds were used to examine that effect. The numerical results of dissipation rate of turbulence kinetic energy show a direct relationship with the increase in rotational speed with maximum values at the blades. It is evident that when (N) increases the turbulence increases especially in radial direction. At highest speed the turbulence dissipation becomes clearly pronounced. It is to be noticed that the dissipated energy near the baffle shows the effect of baffles which induce the turbulence inside the stirred tank.

Fig. 9 shows a horizontal trend draw from the center of the tank toward the tank wall. The intensity of dissipative energy for all speeds located within a distance equal to the blade width which equals to a radius of (15-35 mm). The increase in energy within this distance is non-linear, as shown in the graph, and is followed by a drop along the path towards the wall, before rising again at the baffles. The maximum turbulent dissipation rate reaches maximum before arriving the blades tip for all rotation speeds. This means there is a high turbulence level and high strength vortices at this location. At the blade's tip, the energy level is still high and few millimeters beyond

this tip, it decreases considerably in radial direction. The mean energy dissipation rate (ε) was determined as 0.825, 1.94, and 5.5 m^2/s^3 at the rotational speeds of 180, 240, and 340 rpm, respectively.

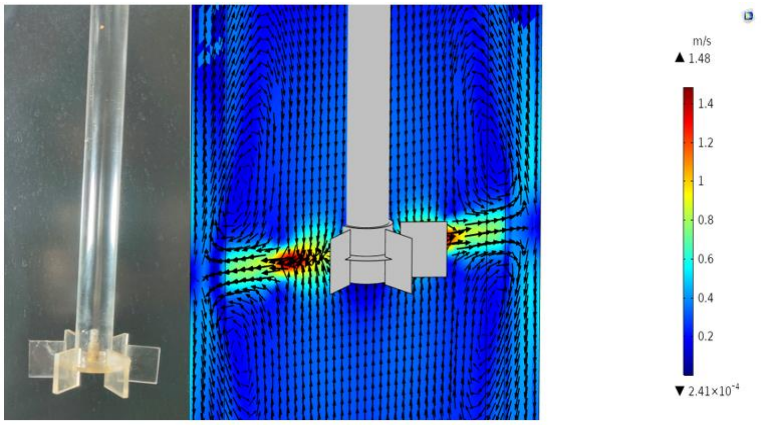

Figure 6: (a) Rushton turbine. (b) Mean velocity vectors for radial impellers at N = 340 rpm.

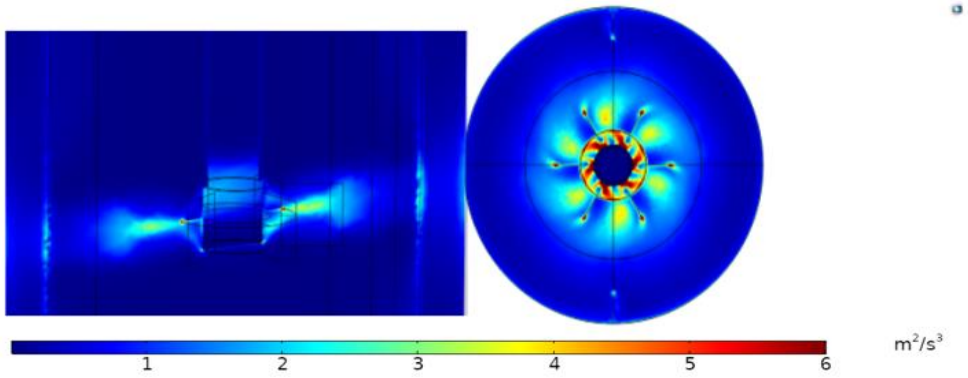

Figure 7: a,b Distribution of turbulence dissipation rate (***ε***) at *N* = 340 rpm.

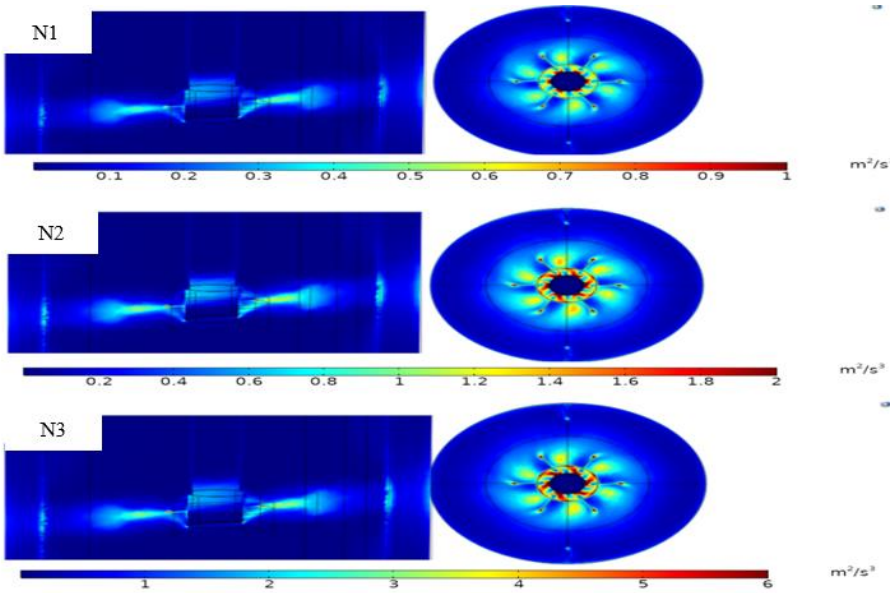

Figure 8: Distribution of turbulence dissipation rate (ε) at N1 =180 rpm, N2 =240 rpm, and N3 =340 rpm.

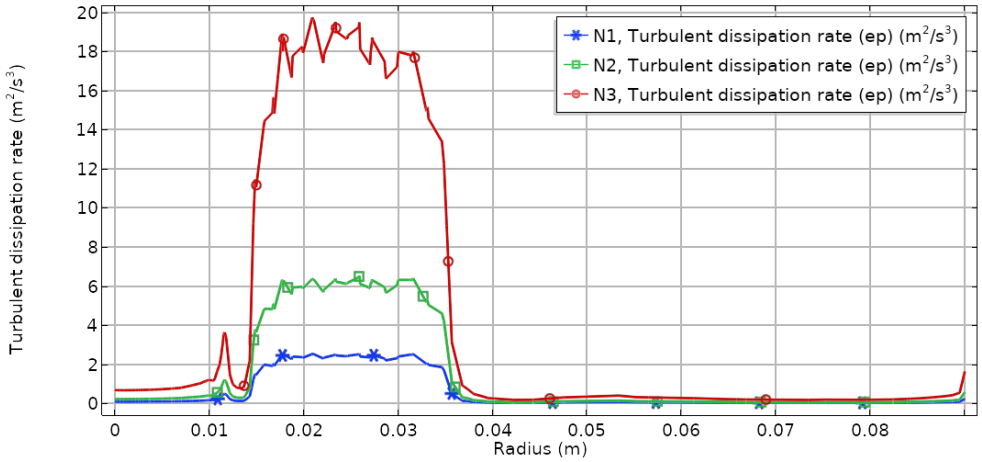

Figure 9: Turbulence dissipation rate (ε) with different rotational speeds at C=H/3.2, N1 =180 rpm, N2 =240 rpm, and N3 =340 rpm.

Fig. 10 represents the effect of rotational speed on the power number (Po) which shows a horizontal curve and slightly decreases with the increase in rotational speed. This is due to the fact that at high rotational speeds which have a Reynold number value of ($Re>10^4$), the flow is described as turbulent and the power number almost constant. The experimental prediction of previous works for turbulent region determined the range of power number is approximately 5-6 [25][26]. The error of predicted power number was within 12.73%. This might be due to the k- ε model's constant parameter, which may not be precise enough for the flow field in stirred tanks. The accuracy of prediction the value of Po tend to increase with the turbulence intensity, which is consistent with the fact that all k-ε models assume a fully developed turbulent regime [27].

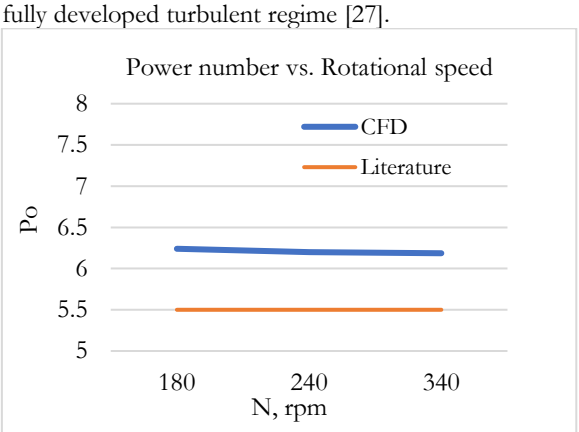

Figure 10: Power number with different rotational speeds.

4.3.1 Bubble breakage behavior

Following the bubble from the point of injection to the point of breakup using a high-speed camera enable us to observe the dynamic behavior of bubble breakage under different turbulent flow conditions. Thus, determining the breakage probability (BP), and the number of fragments (daughter bubbles) produced, and breakage locations relative to the impeller and understanding the governing break-up mechanism.

Based on videos recorded, the spherical mother bubble experiences different scales of deformation which change its shape depending on the region hydrodynamics. At low rotational speeds, the bubble can reach the impeller disk and shift or suck by a low-pressure zone behind the blade. The breakage takes place in the high energy area after the relative scale of deformation as can be seen in Fig. 11, Fig. 12.and Fig. 13. Analysis of the images shows us that the breakage process goes through three stages: oscillation, then elongation, and then break up into binary or multiple fragments of equal or unequal sizes [5][16].

Those figures show different forms of elongation deformation to form a thin thread, dumbbell shape, and long tail with ball connected at one side. For Rushton turbine, side elongation deformation was also observed by Martin [28] and Hasan [21]. The side elongation becomes relatively long and forming a thin thread, this case was also noticed by Solsvik and Jackobsen [29]. The breakage time (define as the time taken from the beginning of the elongation to the first breakage at the low-pressure area behind the blade) shows an inverse relation with power input. For 50 tests, the breakup has an average time of 49.38, 39.84, and 19.8 ms at 180, 240, 340 rpm respectively. The decrease in breakage time was also observed by Zhang [12] and explained this by increasing the eddy velocity due to increasing energy turbulent dissipation rate.

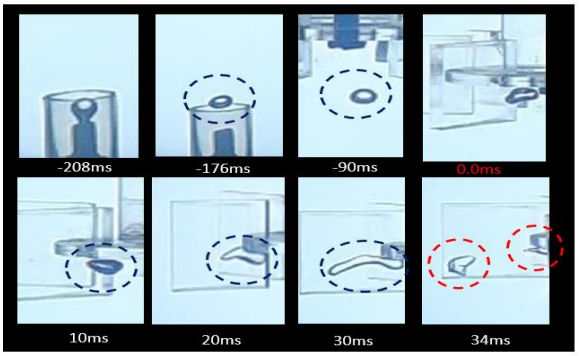

Figure 11: Elongation deformation close to the blades at N=180 rpm.

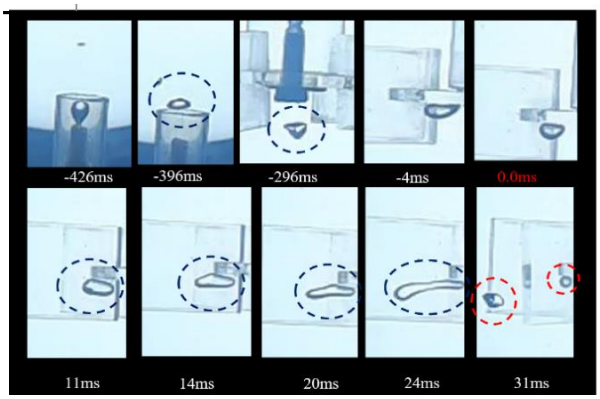

Figure 12: Elongation deformation close to the blades at N=240 rpm.

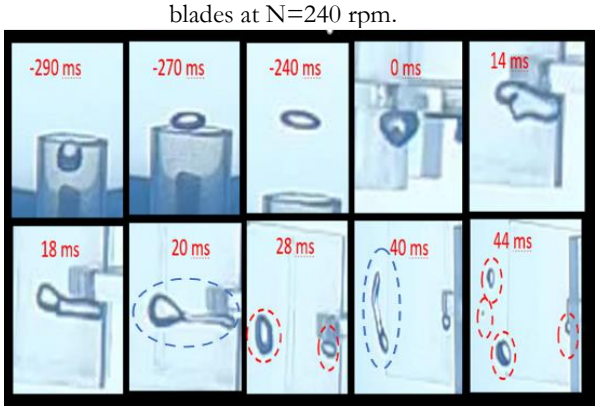

Figure 13: Side ball deformation close to the blades at N = 180 rpm.

4.3.2 Bubble break-up statistics

Methods for increasing bubble break-up are of interest because smaller bubble sizes are generally desired in gas-liquid contact. This section discusses the effect of increasing input power as one of the most effective parameters on the dispersion process. Those results of breakage probability and generated fragments (daughter bubbles) number obtained experimentally for 500 injection tests are determined presented for the Rushton turbine (6RT).

In Fig. 14 and for turbulent conditions, the breakage probability increases as the rotational speed increases. The increase in Bp was about 12.61% when the rotational speed increased from 180 rpm to 340 rpm. Increasing the rotational speed results in an increase in the turbulence intensity and the velocity of generated turbulent eddies as a function of increasing the power input especially around the impeller as shown in Fig. 9. The increase of breakup probability with rotational speed was also observed by Solsvik [11] and Hasan [16] in a stirred tank.

Fig.15, on the other hand, illustrates the average number of fragments (daughter bubbles) generated as a function of rotational speed. Breakage is largely binary and tertiary at lower speeds. However, as the rotational speed increases, it induced cascade breakage and results in a considerable rise in the average number of fragments where multiple breakages dominate. The breakage results in generation multiple fragments due to increasing the power input also reported by several investigations Solsvik and Jakobsen [11], Hasan [16], and Maass and Kraume [30].

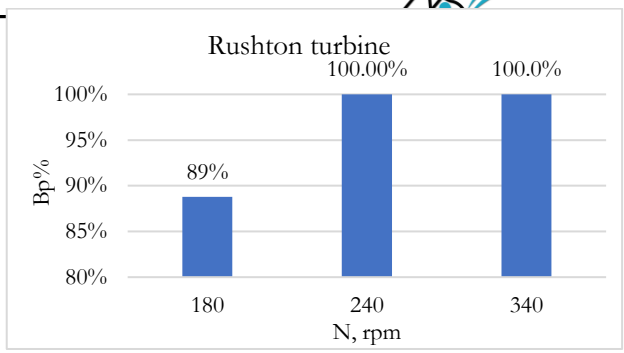

Figure 14: Breakage probability vs. rotational speeds.

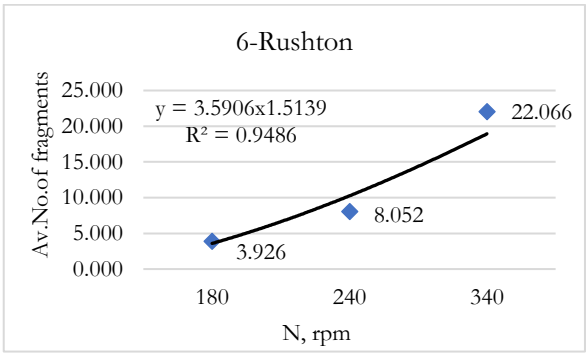

Figure 15: The average number of fragments vs. rotational speeds.

5. Conclusion

Both experimental and numerical method were employed to investigate the hydrodynamics generated by six- flat blades Rushton turbine and its effect on bubble breakage behavior. The predicted flow pattern and power number in addition to the distribution of turbulence energy is consistent with the literatures results. High energy areas are found to occur close to the blade's tip within a distance equal to the blade width of a radius of (15-35 mm) in the radial direction, as well as close to the baffles at the wall. The breakage process occurs in three stages: oscillation, elongation, and break up, and occurs in a high-intensity energy area. The breakage probability (Bp) was found to be increased by 12.61 percent for a mother bubble of 4 mm at 340 rpm, with an average fragmentation of up to 22 fragments. Furthermore, the bubble breakage time was found to decrease by 60% with increasing impeller rotational speed, reaching an average value of 19.8 ms at 340 rpm.

6. References

[1] C. Schaschke, *A dictionary of chemical engineering*. Oxford University Press, 2014.

[2] E. Michaelides, *Particles, bubbles & drops: their motion, heat and mass transfer*. World Scientific, 2006.

[3] W. Resnick and B. Gal-Or, "Gas-liquid dispersions," in *Advances in chemical engineering*, vol. 7, Elsevier, 1968, pp. 295–395.

[4] G. Zhou, *Characteristics of turbulence energy dissipation and liquid-liquid dispersions in an agitated tank*. University of Alberta, 1998.

[5] J. F. Walter and H. W. Blanch, "Bubble break-up in gas—liquid bioreactors: break-up in turbulent flows," *Chem. Eng. J.*, vol. 32, no. 1, pp. B7–B17, 1986.

[6] H. Chen *et al.*, "Interfacial Area Transport Equation for Bubble Coalescence and Breakup: Developments and Comparisons," *Entropy*, vol. 23, no. 9, p. 1106, 2021.
[7] R. Grenville, J. Giacomelli, D. Brown, and G. Padron, "Mixing: Impeller performance in stirred tanks," *Chem. Eng.*, vol. 124, p. 42, Aug. 2017.
[8] S. K. Moon, "Experimental investigation of droplet breakage in the oil-in-water emulsion in a stirred tank." NTNU, 2018.
[9] N. Vankova, S. Tcholakova, N. D. Denkov, I. B. Ivanov, V. D. Vulchev, and T. Danner, "Emulsification in turbulent flow: 1. Mean and maximum drop diameters in inertial and viscous regimes," *J. Colloid Interface Sci.*, vol. 312, no. 2, pp. 363–380, 2007.
[10] B. O. Hasan, "Breakage of drops and bubbles in a stirred tank: A review of experimental studies," *Chinese J. Chem. Eng.*, vol. 25, no. 6, pp. 698–711, 2017.
[11] J. Solsvik and H. A. Jakobsen, "Single air bubble breakup experiments in stirred water tank," *Int. J. Chem. React. Eng.*, vol. 13, no. 4, pp. 477–491, 2015.
[12] H. Zhang, Y. Wang, A. Sayyar, and T. Wang, "Experimental study on breakup of a single bubble in a stirred tank: Effect of gas density and liquid properties," 2021.
[13] J. Solsvik, S. Tangen, and H. A. Jakobsen, "On the constitutive equations for fluid particle breakage," *Rev. Chem. Eng.*, vol. 29, no. 5, pp. 241–356, 2013.
[14] Y. Liao and D. Lucas, "A literature review of theoretical models for drop and bubble breakup in turbulent dispersions," *Chem. Eng. Sci.*, vol. 64, no. 15, pp. 3389–3406, 2009.
[15] B. O. Hasan, M. F. Hamad, H. S. Majdi, and M. M. Hathal, "Experimental characterization of dynamic behavior of single bubble breakage in an agitated tank," *Eur. J. Mech.*, vol. 85, pp. 430–443, 2021.
[16] B. O. Hasan, "Experimental study on the bubble breakage in a stirred tank. Part 1. Mechanism and effect of operating parameters," *Int. J. Multiph. Flow*, vol. 97, pp. 94–108, 2017.
[17] H. A. Alabdly, H. S. Majdi, M. F. Hamad, M. M. Hathal, and B. O. Hasan, "Effect of impeller geometry on bubble breakage and the contributions of different breakage mechanisms in a stirred tank," *Fluid Dyn. Res.*, vol. 52, no. 6, p. 65504, 2020.
[18] F. Krakau and M. Kraume, "3D Single Bubble Breakup Tracking in a Stirred Tank," *Chemie Ing. Tech.*, vol. 91, no. 7, pp. 980–990, 2019.
[19] E. M. Marshall and A. Bakker, "Computational fluid mixing," *Handb. Ind. Mix. Sci. Pract.*, pp. 257–343, 2004.
[20] A. Egedy, T. Varga, and T. Chován, "Investigations on Hydrodynamic in Stirred Vessels for Educational Purposes," *Dep. Process Eng. Univ. Pannonia*, 2011.
[21] A. Ochieng, M. Onyango, and K. Kiriamiti, "Experimental measurement and computational fluid dynamics simulation of mixing in a stirred tank: a review," *S. Afr. J. Sci.*, vol. 105, no. 11, pp. 421–426, 2009.
[22] K. Yapıcı, "Numerical investigation of stirred tank hydrodynamics." 2003.
[23] Y. Saad and M. H. Schultz, "GMRES: A generalized minimal residual algorithm for solving nonsymmetric linear systems," *SIAM J. Sci. Stat. Comput.*, vol. 7, no. 3, pp. 856–869, 1986.
[24] P. Doran, *Bioprocess Engineering Principles*, Seconed. Ed., Academic Press, 2013.
[25] J. H. Rushton, "Power characteristics of mixing impellers part 2," *Chem. Eng. Prog.*, vol. 46, pp. 395–404, 1950.
[26] J. R. Couper, W. R. Penney, J. R. Fair, and S. M. Walas, *Chemical process equipment: selection and design*. Gulf professional publishing, 2005.
[27] D. Marchisio and E. Agostini, "Computational fluid dynamics simulations of flows in stirred tanks: application to bio-reactors," 2019.
[28] M. Martín, F. J. Montes, and M. A. Galán, "Bubbling process in stirred tank reactors I: Agitator effect on bubble size, formation and rising," *Chem. Eng. Sci.*, vol. 63, no. 12, pp. 3212–3222, 2008.
[29] J. Solsvik and H. A. Jakobsen, "Single drop breakup experiments in stirred liquid–liquid tank," *Chem. Eng. Sci.*, vol. 131, pp. 219–234, 2015.
[30] S. Maaß and M. Kraume, "Determination of breakage rates using single drop experiments," *Chem. Eng. Sci.*, vol. 70, pp. 146–164, 2012.